A Spiral Scaffold Underlies Cytoadherent Knobs in *Plasmodium falciparum*-Infected Erythrocytes

Short title: Adherent knobs in malaria-infected erythrocytes

Jean M. Watermeyer[1], Victoria L. Hale[1], Fiona Hackett[2], Daniel K. Clare[1], Erin E. Cutts[3], Ioannis Vakonakis[3], Roland A. Fleck[4], Michael J. Blackman[2] and Helen R. Saibil[1*]

[1]Department of Biological Sciences, Birkbeck, University of London, London, United Kingdom; [2]The Francis Crick Institute, Mill Hill Laboratory, London, United Kingdom; [3]Department of Biochemistry, University of Oxford, Oxford, United Kingdom; [4]Centre for Ultrastructural Imaging, Kings College, London, United Kingdom

* Corresponding author: Helen R. Saibil

Department of Biological Sciences

Birkbeck, University of London

Malet Street, London

WC1E 7HX

Email: h.saibil@mail.cryst.bbk.ac.uk

Tel. +442076316820

Fax. +442076316803

Key Points:

- ***P. falciparum*-generated cytoadherent knobs on infected erythrocytes contain a spiral framework linked to the red cell cytoskeleton**
- **The findings suggest a structural basis for transmission of shear forces in adhesion of infected cells**

Abstract

Much of the virulence of *Plasmodium falciparum* malaria is caused by cytoadherence of infected erythrocytes, which promotes parasite survival by preventing clearance in the spleen. Adherence is mediated by membrane protrusions known as knobs, whose formation depends on the parasite-derived, knob-associated histidine-rich protein (KAHRP). Knobs are required for cytoadherence under flow conditions, and they contain both KAHRP and the parasite-derived erythrocyte membrane protein PfEMP1. Using electron tomography, we have examined the three-dimensional structure of knobs in detergent-insoluble skeletons of *P. falciparum* 3D7 schizonts. We describe a highly organised knob skeleton composed of a spiral structure coated by an electron dense layer underlying the knob membrane. This knob skeleton is connected by multiple links to the erythrocyte cytoskeleton. We used immuno-electron microscopy to locate KAHRP in these structures. The arrangement of membrane proteins in the knobs, visualised by high resolution freeze fracture scanning electron microscopy, is distinct from that in the surrounding erythrocyte membrane, with a structure at the apex that likely represents the adhesion site. Thus, erythrocyte knobs in *P. falciparum* infection contain a highly organised skeleton structure underlying a specialised region of membrane. We propose that the spiral and dense coat organise the cytoadherence structures in the knob, and anchor them into the erythrocyte cytoskeleton. The high density of knobs and their extensive mechanical linkage suggest an explanation for the rigidification of the cytoskeleton in infected cells, and for the transmission to the cytoskeleton of shear forces experienced by adhering cells.

Introduction

Plasmodium falciparum malaria remains one of the leading causes of child deaths globally, with the majority of cases occurring in sub-Saharan Africa and South-East Asia. While chemopreventive and vector control initiatives led to an estimated 42% reduction in mortality rates between 2000-2012, the emergence of artemisinin resistance highlights the importance of continued efforts to understand and interfere with the biology of the parasite [1].

Of the five *Plasmodium* species capable of infecting humans, *P. falciparum* and *P. vivax* are the most prevalent, with *P. falciparum* causing 90% of malaria-related deaths. *P. falciparum*-infected erythrocytes become cytoadherent, causing erythrocyte sequestration in the microvasculature and avoiding clearance of infected cells by the spleen [2]. Much of the virulence of *P. falciparum* malaria has been attributed to this cytoadherence, which impedes blood circulation, and results in severe syndromes such as cerebral or placental malaria [2–4].

The dominant ligand mediating cytoadherence is PfEMP1, a major variable erythrocyte surface antigen of *P. falciparum* which may interact with a number of different host receptors [2,3,5]. Clonal antigenic variation of PfEMP1, encoded by the *var* multi-gene family, has been proposed to be responsible for adherence to different tissues, and hence for variations in disease progression [6,7]. PfEMP1 isoforms are recognised by antibodies that provide variant-specific immunity to *P. falciparum* [3]. One variant, VAR2CSA, which binds to chondroitin sulphate in the placenta causing pregnancy-associated malaria, has been identified as a vaccine target [8]. PfEMP1 is presented on the outside of infected erythrocytes, where it is localised to the surface of membrane protrusions known as knobs [4,9–11]. These knobs appear as prominent bumps on the surface of infected erythrocytes, from the early trophozoite stage

onwards [10,12,13]. PfEMP1 is transported to knobs via Maurer's clefts [14]. Disruption of genes required for PfEMP1 trafficking to the membrane causes dramatic reductions in cytoadherence [15,16]. Loss of the ability to form erythrocyte knobs has been linked with a loss of parasite virulence in primate infections [17], and with reduced cytoadherence *in vitro* [15,18,19].

The formation of the PfEMP1-presenting knobs is dependent on the expression of the parasite-derived knob-associated histidine-rich protein (KAHRP). Erythrocytes infected with KAHRP-negative *P. falciparum* lack knobs and show diminished PfEMP1 presentation and reduced adherence to CD36, ICAM-1 and CSA under flow conditions [18–20]. KAHRP is localised with PfEMP1 in knobs [18,21] where it has been shown by immuno-EM to be associated with an electron-dense (as visualised in heavy-metal stained specimens) layer of material under the membrane, as well as in Maurer's clefts [22,23]. KAHRP is a 59-72 kDa protein (550-657 amino acid residues depending on the variant) containing an N-terminal signal sequence and a PEXEL (*Plasmodium* export element) motif that mediate export into the erythrocyte, a 63-amino-acid histidine-rich (55%) region, and two variable tandem repeat regions [24–26]. Expression of KAHRP has been shown to increase the rigidity of infected erythrocytes, thereby further contributing to cytoadherence-associated virulence [27]. This rigidifying effect on the cytoskeleton is common to a number of exported parasite proteins [15,27]. Use of gene knock-out mutants has revealed that in addition to KAHRP, two genes, those encoding a PHIST domain protein (PFD1170c), and an Hsp40-like DNAJ Type IV protein (PF10_0381), are also important for knob formation [15]. Other parasite proteins that have been shown to associate with knob components, and which may thus form part of the knob structure, include knob-associated Hsp40 [28], the PfEMP1 trafficking protein PfEMP3 [16,28], the large variable surface antigen SURFIN [29], the 2.5 MDa Pf332 antigen [30] and the PHIST domain protein PFE1605w (LyMP) [31,32]. PFE1605w is localised at the cell periphery [33] and has been shown to

be important for cytoadherence but not for knob formation or for surface expression of PfEMP1 [31].

We have examined the architecture of cytoadherent knobs in *P. falciparum* 3D7-infected erythrocytes. By isolating the erythrocyte cytoskeletons of mature schizonts, we have found a distinctive spiral structure with an electron-dense coat underlying the knob membrane. This knob skeleton is anchored into the surrounding erythrocyte cytoskeleton, which connects to the electron-dense coat. Freeze-fracture scanning electron microscopy (SEM) shows that the arrangement of membrane proteins in the knobs is quite distinct from that in the surrounding erythrocyte membrane, with a structure at the apex that may represent the site of adhesion. We propose that the knob skeleton provides a mechanical linkage between the adhesion site and the cytoskeleton.

Methods

P. falciparum culture

P. falciparum 3D7 asexual blood stages were maintained in human erythrocytes in RPMI 1640 medium containing Albumax (Thermo Fisher Scientific, Waltham, MA, U.S.A.), with synchronisation using standard methods [34]. Human blood was obtained with full consent from the UK National Blood Transfusion service, and was used within 2 weeks of receipt. Enrichment of mature schizonts was achieved using Percoll (GE Healthcare, Little Chalfont, UK) as described previously [35].

High pressure freezing and freeze substitution

Mature schizonts were pelleted by centrifugation, mixed with RPMI medium containing brewer's yeast and dextran as a cryoprotectant, and high-pressure frozen in aluminium planchettes using an HPM010 high pressure freezer (BalTec, Reading, UK). This material was freeze-substituted into HM20 resin (Polysciences, Inc., Warrington, PA, U.S.A.) containing 0.2% uranyl acetate. 200-220 nm sections were cut using an EMUC7 ultramicrotome (Leica Camera AG, Wetzlar, Germany) fitted with a diamond knife, and mounted on carbon-coated copper grids. Grids were then coated with 10 nm protein-A gold (Sigma-Aldrich, St. Louis, MO, U.S.A.) as a fiducial marker for tomography.

Preparation of schizont skeletons for negative-stain and cryo-tomography

Cytoskeletons of schizonts and uninfected erythrocytes were prepared *in situ* on carbon-coated copper grids as follows. Grids were glow-discharged, coated with 0.01% poly-*L*-lysine (Sigma-Aldrich) for 30 seconds, washed with water and blotted dry. Grids for cryo-tomography were additionally coated with 10 nm colloidal gold fiducial markers (Sigma-Aldrich). Mature schizonts or uninfected erythrocytes in phosphate-buffered saline (PBS; approx. 20% haematocrit) were applied to the grids, allowed to adhere for 1 minute, then blotted from the back and washed once with PBS. Grids carrying cells were dipped sequentially into lysis buffer (1 mM Tris pH 4.7, 1 mM KCl, 0.2 mM $MgCl_2$), lysis buffer containing 2% Triton X-100, and then lysis buffer without detergent to wash, for 60 seconds in each solution, passing through the meniscus several times. Grids were then either stained with 2% sodium silicotungstate, pH 7.5, blotted and air-dried, or blotted from the back and plunge-frozen in liquid ethane using a manually operated apparatus.

Immunolabelling

Schizont and uninfected erythrocyte skeletons were prepared on grids as described above, then immunolabelled while still wet before staining or plunge-freezing. KAHRP was detected

using monoclonal antibody (mAb) 89 [22] or mAb 18.2 (anti-KAHRP, obtained from the European Malaria Reagent Repository, donated by Dr. Jana McBride), followed by goat anti-mouse secondary antibody doubly conjugated with 10 nm gold and Alexafluor 488 (Thermo Fisher Scientific). Spectrin was detected using antibody ab11751 (Abcam, Cambridge, UK), and gold-conjugated secondary antibody as above. Antibodies were diluted in blocking buffer (0.5% cold water fish skin gelatine (Sigma-Aldrich), 1% normal goat serum (Thermo Fisher Scientific), 0.05% Tween-20 in PBS). Grids were incubated for 30 minutes each in blocking buffer, followed by primary antibody solution, then secondary antibody solution. Grids were washed in PBS between steps, and in low salt buffer before negative staining as described above. For controls, primary antibody was omitted from the second incubation step, or replaced with preimmune serum.

Transmission electron microscopy

Images and tomograms of resin-embedded and negative stained skeletons were collected using an FEI T12 electron microscope with a tungsten filament operated at 120 kV, or an FEI F20 electron microscope operated at 200 kV. A US4000 CCD camera (Gatan, Abingdon, UK) was used for imaging. Dual-axis tomograms were collected using a dual-tilt tomography holder (E.A. Fischione Instruments, Inc., Export, PA, U.S.A.).

Cryo-tomograms were collected from vitrified specimens 100-300 nm thick using a Polara electron microscope operated at 300 kV (FEI Company, Hillsboro, OR, U.S.A.), equipped with a Quantum energy filter and a K2 direct electron detector (Gatan). Zero loss filtering was carried out using a 20 eV slit width. Images were collected in electron counting mode with dose fractionation, using 3-6-second exposures with 6-20 subframes per exposure. Total exposures were 60-110 electrons per square Angstrom ($e^-/Å^2$) for cryo-tomograms and 200-270 $e^-/Å^2$ for negative-stain dual-axis tomograms. Tomographic tilt-series collection was controlled using Serial EM [36].

Image processing

Tomographic reconstruction and subframe alignment were carried out using IMOD [37]. 5 or 10 nm gold beads were used as fiducial markers, and some tomograms were aligned by patch tracking. Gold particles in tomographic reconstructions were detected automatically using IMOD findbeads3d, knobs were modelled using 3dmod, and the relative spatial distribution of gold and knobs was calculated using IMOD MTK [37]. The average densities of gold beads calculated by MTK for individual tomograms were combined by weighting the tomogram average according to the number of knobs present. Gold beads in images of immunolabelled material were counted automatically using ImageJ. Tomograms were denoised for display using nonlinear anisotropic diffusion (NAD) filtering.

Freeze-fracture scanning electron microscopy

Mature schizonts were concentrated by centrifugation, high-pressure frozen as above without additional cryo-protectant, then fractured at -110 °C and multi-axis rotary coated at high vacuum with a 4 nm layer of chromium using a BAF060 freeze fracture system fitted with a VCT100 vacuum cryo transfer system (BalTec). Samples were imaged under cryo-conditions using a specialised semi in-lens cryo-SEM (JSM-7401F, JEOL (UK) Ltd, Welwyn Garden City, UK) equipped with a cold-source field emission gun, beam deceleration and an energy filter. Images were collected using low beam landing energy (1.2 kV) at 37000 - 60000x magnification and a working distance of 4-5.4 nm.

Database depositions

Representative tomograms have been deposited in the Electron Microscopy Data Bank, codes EMD-3116, EMD-3117, EMD-3122 and EMD-3123.

Results

Architecture of *P. falciparum*-induced erythrocyte knobs

During blood stage development of the parasite, the most evident change to the erythrocyte cell surface is the appearance of the cytoadherent knobs [10,12,13]. In order to characterise knob structure, we processed synchronised late schizonts by high-pressure freezing and freeze substitution and examined sections of this material by electron microscopy. Knobs are visible as prominent protrusions on the surface of the erythrocyte membrane (Figure 1), as previously observed [10,18,23,38–45]. A layer of electron-dense material approximately 13 nm thick lies under the membrane in the knobs, about 10 nm below the membrane bilayer (Figure 1). It thus occupies a similar position to the erythrocyte cytoskeleton relative to the membrane [46]. The electron-dense material follows the shape of the knob in three dimensions (3D), forming cup-shaped structures ranging from 40-145 nm in diameter and averaging 50 nm in height (43 knobs examined).

A spiral structure underlies knobs

To obtain a more detailed view of the knob structure, we examined detergent-insoluble schizont skeletons by negative-stain electron microscopy. Knobs are visible as dark patches in the erythrocyte cytoskeleton, 70-100 nm in diameter (Figure 2). When this material is examined by electron tomography, structural components are resolved in 3D rather than being projected onto a single plane. In the resulting 3D reconstructions, knobs can clearly be seen to contain spirals made up of a stain-excluding filament 2-3 nm wide (Video S1). Figure 3 A-C shows slices of these spirals at different depths through the knobs. Tracing these structures in 3D reveals that each knob contains a spiral filament that coils into a shallow cone (Figure 3D,E, Video S1). Spirals turn anti-clockwise as viewed from the cytoplasmic

(concave) side (Figure 3D,E, Figure S2). The spacing between turns of the filament varies from 5-12 nm, and the gaps between turns contain a radiating structure with major radial features spaced approximately 4 nm apart (Figure 3A). A layer of more diffuse material, also having a radiating pattern, coats the upper surface of the conical frame formed by the spiral (viewed in different orientations in Figure 3C,F). When viewed from the side, this coating coincides with the cup-shaped structure seen as an electron-dense layer in resin-embedded sections (compare Figure 4A,B). This structure lies between the 2-3 nm spiral filament and the membrane, in cases where detergent extraction was incomplete (Figure 4B). The whole spiral-plus-coat structure (which we will refer to together as the knob skeleton) is 20-50 nm in height, similar to what was seen for resin-embedded material, suggesting that the negative stain procedure did not cause noticeable flattening. Knob density in the cytoskeleton was 11.8 +/- 5.1 knobs/μm^2, which is similar to that reported for *P. falciparum* strains subjected to long-term *in vitro* culture as in this study [47].

Knobs are embedded in the cytoskeleton and have a discontinuity at their apex

To examine the cytoskeleton in the hydrated state, we prepared frozen-hydrated schizont skeletons and imaged these by cryo-electron tomography (Figures 4C, 5; Video S3). Cytoskeleton and knobs can be seen clearly in the resulting cryo-tomograms (Figure 5A,C). It was possible to partially trace the path of the spirals, and to identify the coat on the outside of the spiral cone (Figure 5C). The coat coincides with the electron-dense layer in high-pressure frozen material and with the diffuse layer in negative stain (Figure 4). In cases where knobs present clear side views in the resulting cryo-tomograms, there is a discontinuity at the apex of the knob, with a break in the residual membrane in preparations where detergent extraction was incomplete (Figure 4C). This suggests a difference in membrane properties at this point, which could indicate the presence of specialised transmembrane components. In Figure 5D, a model of the 3D structure traced from the 3D reconstruction (see Video S3) is

superposed on a section of the density. Cytoskeletal filaments (blue) connect to the outside of the coat layer (magenta, Figure 5D). Points of contact between the cytoskeleton and coat layer (yellow spheres) are apparent over the whole surface of the coat layer, but most connections occur around the knob base (Figure 5E). No cytoskeletal material can be seen passing underneath the knobs (Video S3) in tomograms where the two apposed layers of the cytoskeleton, arising from the upper and lower cell surfaces, can be adequately distinguished. An anti-spectrin antibody, recognising the erythroid spectrin alpha chain SH3 domain, labelled the erythrocyte skeleton of schizonts as expected, but labelling was almost completely excluded from regions within 50 nm of the centres of knobs (Figure S4). This suggests that spectrin, the major erythrocyte cytoskeletal building block, is excluded from the inside of the knobs, which were 70-100 nm in diameter. This supports the model described in Figure 5D,E, in which spectrin connects to the outer edges of knobs without passing underneath them. Importantly, outside of the knobs, there is no obvious qualitative difference in cytoskeleton structure between infected and uninfected erythrocyte skeletons (Figure 5A,B).

KAHRP is in the diffuse layer coating the spiral

Previous studies have demonstrated that the material underlying knobs contains KAHRP [22,23]. To locate KAHRP in the schizont skeletons, we used monoclonal antibodies (mAb) against KAHRP. Labelling was detected by negative-stain and cryo-electron tomography using a gold-conjugated secondary antibody (Figure 6). Skeletons labelled with anti-KAHRP antibody 18.2 (Figure 6A,B) have gold beads clustered over the surface (Figure 6C,D), separated from the spiral by 10-60 nm (Figure 6E). Uninfected erythrocyte skeletons showed no labelling under identical conditions (Figure S5). A similar pattern of labelling was seen using anti-KAHRP antibody 89, which recognizes a different part of the KAHRP sequence (Figure S6). The epitope for mAb 18.2 is located in residues 282-362 of KAHRP, while that for mAb 89 lies

within residues 424-539 (Figure S6) [48]. These findings are in agreement with the earlier work and confirm that the knob skeletons contain KAHRP.

Membrane proteins are reorganised at knobs.

To examine the distribution of proteins in the knob membrane, we used a custom-optimised system combining cryo-scanning electron microscopy (cryo-SEM) at ~2 nm resolution, with freeze-fracture. Freeze-fracture allows examination of the individual leaflets of the membrane bilayer, while this system facilitates visualisation over a fractured surface containing many thousands of schizonts at high magnification (Figure 7). Knobs appear as pits in the E-face (the inside of the outer membrane leaflet; Figure 7A) or protrusions in the P-face (the outside of the inner membrane leaflet; Figure 7B). Membrane proteins in the E-face are arranged in a mesh pattern that closely resembles the mesh of the cytoskeleton in dimensions and arrangement; knob protrusions show a circular clearing in this pattern with membrane proteins only remaining at the apex (Figure 7A). The dimensions of individual globular components in the pattern of membrane proteins range between 8-25 nm, including the 4 nm chromium coating. Membrane proteins in the P-face are smaller (approx. 5-10 nm) and appear less organised than in the E-face. However, a circular zone of clearing is also evident around the edges of the knob protrusions, similar to what was seen previously by low resolution freeze-fracture SEM of the P-face (Figure 7B)[19,39]. These findings demonstrate that the knob membrane has a distinct distribution of membrane proteins from the surrounding erythrocyte membrane, including a discrete structure at the apex.

Discussion

We have examined the cytoadherent knobs in *P. falciparum*-infected erythrocytes and have described a knob skeleton, containing a spiral structure, underlying the membrane protrusions (Figures 3,4). This structure is described schematically in Figure 7C. Armed with the present data, one can detect hints of the spiral structure in previously published images of purified knobs [49]. Our use of 3D imaging of schizont skeletons facilitated the interpretation of these structures as conical spirals.

The outer coat of the knob skeleton makes multiple connections to the surrounding erythrocyte cytoskeleton (Figure 5C-E; Video S3). These mechanical linkages suggest a means by which the shear forces involved in cytoadhesion by the knobs under flow conditions could be transmitted to the surrounding cytoskeleton (e.g., as discussed by [18]). A spiral support at the point of attachment might function in a spring-like fashion to absorb sudden changes in mechanical stress. Intrinsic flexibility in the structure that would support this idea is suggested by the variations observed in spacing between turns of the spiral.

Insertion of KAHRP-containing knobs into the cytoskeleton may also explain the rigidifying effect of KAHRP on the infected erythrocyte [27]. Knobs are present at high density on the surface of infected erythrocytes, and the numerous connections between the coat layer and the surrounding cytoskeleton are likely to have a significant impact on cytoskeletal mechanics. In clinical isolates, knob densities can reach up to four times what we observed in this laboratory strain [47]. These findings support the mechanism proposed in a recent modelling analysis for the rigidifying effect of the knobs on the erythrocyte cytoskeleton [50]. Spectrin tetramers are capable of stretching to 194 nm in length [51], which would allow for

knob intercalation into the cytoskeleton mesh without further modification. It has been reported that the red cell cytoskeleton is gradually dismantled as the intracellular parasite develops [42,52,53], and it is possible that some cytoskeletal connections are broken during knob formation. However, in this study, which used highly synchronised, mature schizont preparations, no differences in cytoskeletal structure outside of the knobs were observed between uninfected erythrocyte skeletons and those from mature schizonts. These findings are not consistent with the notion of progressive degradation of the cytoskeleton.

Knobs are thought to comprise a complex of the cytoadherent ligand PfEMP1, KAHRP, other parasite-derived proteins and erythrocyte cytoskeleton components, such as spectrin, F-actin and ankyrin-R [32,54–62]. A central fragment of KAHRP containing lysine-rich repeat regions forms electron-dense patches under the membrane in resealed erythrocytes [48], and full-length KAHRP expressed in *E. coli* forms clusters that associate with spectrin [57]. Our immunolabelling (Figure 6) strengthens earlier evidence localising KAHRP to the electron-dense layer underlying knobs [22,23].

The distinctive spiral structure in the knobs (Figure 3) bears a striking resemblance to the structures formed by eukaryotic ESCRT-III proteins involved in ATP-driven intraluminal vesicle budding and membrane scission in mammalian and yeast cells [63,64, 65–67]. ESCRT-III proteins comprise alpha-helical bundles that assemble into a membrane-associated spiral [63]. While no homology could be detected between ESCRT-III proteins and any of the known components of knobs (Supporting Information S7), it is noteworthy that they both involve spiral structures of very similar appearance in membrane deformation. Only low levels of native ESCRT-III proteins have been detected in erythrocytes [68]. By comparison, knobs are present at high density in infected erythrocytes and also contain high concentrations of KAHRP [12]. The *P. falciparum* genome encodes five homologues of eukaryotic ESCRT-III

proteins (PF08_0064, PFI00300w, PFL2090c, PF14_0397 and PF11_0434; Supporting Information S7), all of which are expressed in the blood stages. However none of these is known or predicted to be exported to the erythrocyte cytoplasm (Supporting Information S7). None of the knob-associated proteins is known to have ATPase activity, as might be expected for ESCRT-III complexes.

The erythrocyte membrane is modified considerably during *P. falciparum* infection by the insertion of parasite-derived proteins, including PfEMP1, as well as by changes in phosphorylation of cytoskeleton-associated proteins [69–72]. Phosphorylation of erythrocyte band 3 during infection has been shown to cause uncoupling of this cytoskeleton-organising transmembrane protein from the cytoskeleton [73]. We observed a rearrangement of transmembrane proteins at knobs by high-resolution, freeze-fracture cryo-SEM (Figure 7A,B). This is consistent with a role for knobs in organising and presenting transmembrane ligands on the erythrocyte surface [18,19]. In the E-face, knobs form prominent clearings in a network of membrane proteins, which are absent from all but the knob apex. A discontinuity was also observed at the apex of knobs in cryo-tomograms, consistent with a difference in the properties of the membrane at this point (Figure 4). Given that PfEMP1 has been clearly localised to the surface of knobs [9,19], and that adhesion appears to occur at the apex of knobs in sections of infected cells adhering to the epithelial surface [19], it seems likely that a PfEMP1-containing adhesive structure is located at the knob apex. Outside of the knobs, the network pattern of membrane proteins seen in the E-face by freeze-fracture SEM suggests that these may be cytoskeleton-associated, possibly band 3 or glycophorins (although there is some evidence that band 3 partitions preferentially with the P-face during fracture of uninfected erythrocytes [74,75]). Altered membrane protein distribution at knobs is less marked in the P-face, although there are clearings around knobs similar to those observed previously by SEM of freeze-fracture replicas [19,39].

In conclusion, we have shown that erythrocyte knobs in *P. falciparum* infection contain a highly organised coated spiral structure underlying a specialised region of membrane (Figure 7C). The application of electron tomography to schizont skeletons has revealed this previously undescribed knob skeletal framework. The observation of multiple connections between the knob skeleton and the erythrocyte cytoskeleton suggests a mechanical explanation for the cytoadherence-enhancing effects of knobs as well as for the reduction in cytoskeletal flexibility caused by knob components. The discovery of these structures suggests new avenues of research to elucidate the roles of individual components of the knob structure in antigen presentation and adherence.

Acknowledgements

We thank Kirsty MacLellan-Gibson for her assistance, and Andrew Osborne, Andrea Nans, Richard Hayward and Giulia Zanetti for helpful discussions. This work was supported by Medical Research Council Project Grant G1100013 (HRS, MJB, RAF), the EU FP7 NoE EviMalAR (MJB), the Wellcome Trust (088497/Z/09/Z (IV); PhD studentship (EEC); equipment grants 101488, 079605 and 086018 (HRS, MJB, RAF)) and the BBSRC (CASE PhD studentship BB/F016948/1 (VLH); equipment grant BB/L014211 (HRS)). We thank David Houldershaw and Richard Westlake for computing support, Peter Rosenthal for providing access to some facilities at the Francis Crick Mill Hill Laboratory, and Prof. Diane W. Taylor for her kind gift of anti-KAHRP mAb 89; mAb 18.2 was obtained from The European Malaria Reagent Repository (http://www.malariaresearch.eu).

Authorship contributions

Contribution: J.M.W., I.V., R.A.F., M.J.B. and H.R.S. designed the research and wrote the manuscript; J.M.W, V.L.H, F.H, D.K.C and E.E.C. performed the research and collected data; J.M.W., V.L.H, I.V., R.A.F., M.J.B. and H.R.S. analysed and interpreted the data.

Disclosure of conflicts of interest

The PhD studentship of VLH was partly funded by Gatan, but the funders were not involved in planning the research. The authors declare that there were no other conflicts of interest.

References

1. World Health Organisation. World Malaria Report 2013. France: World Health Organisation; 2013.

2. Miller LH, Baruch DI, Marsh K, Doumbo OK. The pathogenic basis of malaria. *Nature*. 2002;415(6872):673–9.

3. Chan J-A, Fowkes FJI, Beeson JG. Surface antigens of *Plasmodium falciparum*-infected erythrocytes as immune targets and malaria vaccine candidates. *Cell. Mol. Life Sci.* 2014;71(19):3633–57.

4. Cooke B, Coppel R, Wahlgren M. Falciparum malaria: sticking up, standing out and out-standing. *Parasitol. Today*. 2000;16(10):416–20.

5. Ho M, White NJ. Molecular mechanisms of cytoadherence in malaria. *Am. J. Physiol.* 1999;276(6 Pt 1):C1231–42.

6. Smith JD, Chitnis CE, Craig AG, et al. Switches in expression of Plasmodium falciparum var genes correlate with changes in antigenic and cytoadherent phenotypes of infected erythrocytes. *Cell*. 1995;82(1):101–110.

7. Flick K, Chen Q. *var* genes, PfEMP1 and the human host. *Mol. Biochem. Parasitol.* 2004;134(1):3–9.

8. Hviid L. The role of *Plasmodium falciparum* variant surface antigens in protective immunity and vaccine development. *Hum. Vaccin.* 2010;6(1):84–9.

9. Baruch DI, Pasloske BL, Singh HB, et al. Cloning the *P. falciparum* gene encoding PfEMP1, a malarial variant antigen and adherence receptor on the surface of parasitized human erythrocytes. *Cell.* 1995;82(1):77–87.

10. Tilley L, Hanssen E. A 3D view of the host cell compartment in *P. falciparum*-infected erythrocytes. *Transfus. Clin. Biol.* 2008;15(1-2):72–81.

11. Nakamura K, Hasler T, Morehead K, Howard RJ, Aikawa M. *Plasmodium falciparum*-infected erythrocyte receptor(s) for CD36 and thrombospondin are restricted to knobs on the erythrocyte surface. *J. Histochem. Cytochem.* 1992;40(9):1419–22.

12. Kilejian A. Characterization of a protein correlated with the production of knob-like protrusions on membranes of erythrocytes infected with *Plasmodium falciparum*. *Proc. Natl. Acad. Sci. U. S. A.* 1979;76(9):4650–3.

13. Nagao E, Kaneko O, Dvorak JA. *Plasmodium falciparum*-infected erythrocytes: qualitative and quantitative analyses of parasite-induced knobs by atomic force microscopy. *J. Struct. Biol.* 2000;130(1):34–44.

14. Kriek N, Tilley L, Horrocks P, et al. Characterization of the pathway for transport of the cytoadherence-mediating protein, PfEMP1, to the host cell surface in malaria parasite-infected erythrocytes. *Mol. Microbiol.* 2003;50(4):1215–27.

15. Maier AG, Rug M, O'Neill MT, et al. Exported proteins required for virulence and rigidity of *Plasmodium falciparum*-infected human erythrocytes. *Cell.* 2008;134(1):48–61.

16. Waterkeyn JG, Wickham ME, Davern KM, et al. Targeted mutagenesis of *Plasmodium falciparum* erythrocyte membrane protein 3 (PfEMP3) disrupts cytoadherence of malaria-infected red blood cells. *EMBO J.* 2000;19(12):2813–23.

17. Langreth SG, Peterson E. Pathogenicity, stability, and immunogenicity of a knobless clone of *Plasmodium falciparum* in Colombian owl monkeys. *Infect. Immun.* 1985;47(3):760–6.

18. Crabb BS, Cooke BM, Reeder JC, et al. Targeted gene disruption shows that knobs enable malaria-infected red cells to cytoadhere under physiological shear stress. *Cell.* 1997;89(2):287–96.

19. Horrocks P, Pinches RA, Chakravorty SJ, et al. PfEMP1 expression is reduced on the surface of knobless *Plasmodium falciparum* infected erythrocytes. *J. Cell Sci.* 2005;118(Pt 11):2507–18.

20. Cooke BM, Glenister FK, Mohandas N, Coppel RL. Assignment of functional roles to parasite proteins in malaria-infected red blood cells by competitive flow-based adhesion assay. *Br. J. Haematol.* 2002;117(1):203–11.

21. Ganguly AK, Ranjan P, Kumar A, Bhavesh NS. Dynamic association of PfEMP1 and KAHRP in knobs mediates cytoadherence during *Plasmodium* invasion. *Sci. Rep.* 2015;5:8617.

22. Taylor DW, Parra M, Chapman GB, et al. Localization of *Plasmodium falciparum* histidine-rich protein 1 in the erythrocyte skeleton under knobs. *Mol. Biochem. Parasitol.* 1987;25(2):165–74.

23. Culvenor JG, Langford CJ, Crewther PE, et al. *Plasmodium falciparum*: identification and localization of a knob protein antigen expressed by a cDNA clone. *Exp. Parasitol.* 1987;63(1):58–67.

24. Triglia T, Stahl HD, Crewther PE, et al. The complete sequence of the gene for the knob-associated histidine-rich protein from Plasmodium falciparum. *EMBO J.* 1987;6(5):1413–9.

25. Hirawake H, Kita K, Sharma YD. Variations in the C-terminal repeats of the knob-associated histidine-rich protein of *Plasmodium falciparum*. *Biochim. Biophys. Acta*. 1997;1360(2):105–8.

26. Marti M, Good RT, Rug M, Knuepfer E, Cowman AF. Targeting malaria virulence and remodeling proteins to the host erythrocyte. *Science*. 2004;306(5703):1930–3.

27. Glenister FK, Coppel RL, Cowman AF, Mohandas N, Cooke BM. Contribution of parasite proteins to altered mechanical properties of malaria-infected red blood cells. *Blood*. 2002;99(3):1060–1063.

28. Acharya P, Chaubey S, Grover M, Tatu U. An exported heat shock protein 40 associates with pathogenesis-related knobs in *Plasmodium falciparum* infected erythrocytes. *PLoS One*. 2012;7(9):e44605.

29. Winter G, Kawai S, Haeggström M, et al. SURFIN is a polymorphic antigen expressed on *Plasmodium falciparum* merozoites and infected erythrocytes. *J. Exp. Med.* 2005;201(11):1853–63.

30. Hinterberg K, Scherf A, Gysin J, et al. *Plasmodium falciparum*: the Pf332 antigen is secreted from the parasite by a brefeldin A-dependent pathway and is translocated to the erythrocyte membrane via the Maurer's clefts. *Exp. Parasitol.* 1994;79(3):279–91.

31. Proellocks NI, Herrmann S, Buckingham DW, et al. A lysine-rich membrane-associated PHISTb protein involved in alteration of the cytoadhesive properties of *Plasmodium falciparum*-infected red blood cells. *FASEB J.* 2014;28(7):3103–13.

32. Oberli A, Slater LM, Cutts E, et al. A *Plasmodium falciparum* PHIST protein binds the virulence factor PfEMP1 and comigrates to knobs on the host cell surface. *FASEB J.* 2014;

33. Tarr SJ, Moon RW, Hardege I, Osborne AR. A conserved domain targets exported PHISTb family proteins to the periphery of *Plasmodium* infected erythrocytes. *Mol. Biochem. Parasitol.* 2014;196(1):29–40.

34. Yeoh S, O'Donnell RA, Koussis K, et al. Subcellular discharge of a serine protease mediates release of invasive malaria parasites from host erythrocytes. *Cell*. 2007;131(6):1072–83.

35. Harris PK, Yeoh S, Dluzewski AR, et al. Molecular identification of a malaria merozoite surface sheddase. *PLoS Pathog.* 2005;1(3):241–51.

36. Mastronarde DN. Automated electron microscope tomography using robust prediction of specimen movements. *J. Struct. Biol.* 2005;152(1):36–51.

37. Mastronarde DN. Dual-axis tomography: an approach with alignment methods that preserve resolution. *J. Struct. Biol.* 1997;120(3):343–52.

38. Hanssen E, McMillan PJ, Tilley L. Cellular architecture of Plasmodium falciparum-infected erythrocytes. *Int. J. Parasitol.* 2010;40(10):1127–35.

39. Allred DR, Gruenberg JE, Sherman IW. Dynamic rearrangements of erythrocyte membrane internal architecture induced by infection with *Plasmodium falciparum*. *J. Cell Sci.* 1986;81:1–16.

40. Aikawa M. Morphological changes in erythrocytes induced by malarial parasites. *Biol. Cell.* 1988;64(2):173–81.

41. Sachanonta N, Chotivanich K, Chaisri U, et al. Ultrastructural and real-time microscopic changes in *P. falciparum*-infected red blood cells following treatment with antimalarial drugs. *Ultrastruct. Pathol.* 2011;35(5):214–25.

42. Cyrklaff M, Sanchez CPC, Kilian N, et al. Hemoglobins S and C interfere with actin remodeling in *Plasmodium falciparum*-infected erythrocytes. *Science*. 2011;334(6060):1283–6.

43. Frankland S, Adisa A, Horrocks P, et al. Delivery of the malaria virulence protein PfEMP1 to the erythrocyte surface requires cholesterol-rich domains. *Eukaryot. Cell*. 2006;5(5):849–60.

44. Bannister LH, Hopkins JM, Fowler RE, Krishna S, Mitchell GH. A brief illustrated guide to the ultrastructure of *Plasmodium falciparum* asexual blood stages. *Parasitol. Today*. 2000;16(10):427–33.

45. Wickham ME, Rug M, Ralph SA, et al. Trafficking and assembly of the cytoadherence complex in *Plasmodium falciparum*-infected human erythrocytes. *EMBO J.* 2001;20(20):5636–49.

46. Shahrokh Z, Verkman AS, Shohet SB. Distance between skeletal protein 4.1 and the erythrocyte membrane bilayer measured by resonance energy transfer. *J. Biol. Chem.* 1991;266(18):12082–9.

47. Quadt KA, Barfod L, Andersen D, et al. The density of knobs on *Plasmodium falciparum*-infected erythrocytes depends on developmental age and varies among isolates. *PLoS One*. 2012;7(9):e45658.

48. Kilejian A, Rashid MA, Parra M, Yang YF. Sequence of the knob protein of *Plasmodium falciparum* recognized by a monoclonal antibody. *Mol. Biochem. Parasitol.* 1991;48(2):231–3.

49. Chishti AH, Andrabi KI, Derick LH, Palek J, Liu S-CC. Isolation of skeleton-associated knobs from human red blood cells infected with malaria parasite *Plasmodium falciparum*. *Mol. Biochem. Parasitol.* 1992;52(2):283–287.

50. Zhang Y, Huang C, Kim S, et al. Multiple stiffening effects of nanoscale knobs on human red blood cells infected with Plasmodium falciparum malaria parasite. *Proc. Natl. Acad. Sci. U. S. A.* 2015;112(19):6068–6073.

51. Nans A, Mohandas N, Stokes DL. Native ultrastructure of the red cell cytoskeleton by cryo-electron tomography. *Biophys. J.* 2011;101(10):2341–50.

52. Millholland MG, Chandramohanadas R, Pizzarro A, et al. The malaria parasite progressively dismantles the host erythrocyte cytoskeleton for efficient egress. *Mol. Cell. Proteomics*. 2011;10(12):M111.010678.

53. Shi H, Liu Z, Li A, et al. Life cycle-dependent cytoskeletal modifications in *Plasmodium falciparum* infected erythrocytes. *PLoS One*. 2013;8(4):e61170.

54. Weng H, Guo X, Papoin J, et al. Interaction of *Plasmodium falciparum* knob-associated histidine-rich protein (KAHRP) with erythrocyte ankyrin R is required for its attachment to the erythrocyte membrane. *Biochim. Biophys. Acta*. 2014;1838(1):185–92.

55. Mayer C, Slater L, Erat MC, Konrat R, Vakonakis I. Structural analysis of the *Plasmodium falciparum* erythrocyte membrane protein 1 (PfEMP1) intracellular domain reveals a conserved interaction epitope. *J. Biol. Chem.* 2012;287(10):7182–9.

56. Voigt S, Hanspal M, LeRoy PJ, et al. The cytoadherence ligand *Plasmodium falciparum* erythrocyte membrane protein 1 (PfEMP1) binds to the *P. falciparum* knob-associated histidine-rich protein (KAHRP) by electrostatic interactions. *Mol. Biochem. Parasitol.* 2000;110(2):423–8.

57. Oh SS, Voigt S, Fisher D, et al. *Plasmodium falciparum* erythrocyte membrane protein 1 is anchored to the actin-spectrin junction and knob-associated histidine-rich protein in the erythrocyte skeleton. *Mol. Biochem. Parasitol.* 2000;108(2):237–247.

58. Waller KL, Nunomura W, Cooke BM, Mohandas N, Coppel RL. Mapping the domains of the cytoadherence ligand *Plasmodium falciparum* erythrocyte membrane protein 1 (PfEMP1) that bind to the knob-associated histidine-rich protein (KAHRP). *Mol. Biochem. Parasitol.* 2002;119(1):125–9.

59. Cooke BM, Mohandas N, Coppel RL. Malaria and the red blood cell membrane. *Semin. Hematol.* 2004;41(2):173–188.

60. Kilejian A, Rashid MA, Aikawa M, Aji T, Yang YF. Selective association of a fragment of the knob protein with spectrin, actin and the red cell membrane. *Mol. Biochem. Parasitol.* 1991;44(2):175–81.

61. Pei X, An X, Guo X, et al. Structural and functional studies of interaction between *Plasmodium falciparum* knob-associated histidine-rich protein (KAHRP) and erythrocyte spectrin. *J. Biol. Chem.* 2005;280(35):31166–71.

62. Waller KL, Cooke BM, Nunomura W, Mohandas N, Coppel RL. Mapping the binding domains involved in the interaction between the *Plasmodium falciparum* knob-associated histidine-rich protein (KAHRP) and the cytoadherence ligand *P. falciparum* erythrocyte membrane protein 1 (PfEMP1). *J. Biol. Chem.* 1999;274(34):23808–23813.

63. Henne WM, Stenmark H, Emr SD. Molecular mechanisms of the membrane sculpting ESCRT pathway. *Cold Spring Harb. Perspect. Biol.* 2013;5(9):a016766.

64. Cashikar AG, Shim S, Roth R, et al. Structure of cellular ESCRT-III spirals and their relationship to HIV budding. *Elife*. 2014;e02184.

65. Bissig C, Gruenberg J. ALIX and the multivesicular endosome: ALIX in Wonderland. *Trends Cell Biol.* 2014;24(1):19–25.

66. Lata S, Schoehn G, Solomons J, et al. Structure and function of ESCRT-III. *Biochem. Soc. Trans.* 2009;37(Pt 1):156–60.

67. Solomons J, Sabin C, Poudevigne E, et al. Structural basis for ESCRT-III CHMP3 recruitment of AMSH. *Structure*. 2011;19(8):1149–59.

68. D'Alessandro A, Righetti PG, Zolla L. The red blood cell proteome and interactome: an update. *J. Proteome Res.* 2010;9(1):144–63.

69. Mbengue A, Yam XY, Braun-Breton C. Human erythrocyte remodelling during *Plasmodium falciparum* malaria parasite growth and egress. *Br. J. Haematol.* 2012;157(2):171–9.

70. Pantaleo A, Ferru E, Vono R, et al. New antimalarial indolone-N-oxides, generating radical species, destabilize the host cell membrane at early stages of *Plasmodium falciparum growth*: role of band 3 tyrosine phosphorylation. *Free Radic. Biol. Med.* 2012;52(2):527–36.

71. Pantaleo A, Ferru E, Carta F, et al. Analysis of changes in tyrosine and serine phosphorylation of red cell membrane proteins induced by *P. falciparum growth*. *Proteomics*. 2010;10(19):3469–79.

72. Roggwiller E, Bétoulle ME, Blisnick T, Braun-Breton C. A role for erythrocyte band 3 degradation by the parasite gp76 serine protease in the formation of the parasitophorous vacuole during invasion of erythrocytes by *Plasmodium falciparum*. *Mol. Biochem. Parasitol.* 1996;82(1):13–24.

73. Ferru E, Giger K, Pantaleo A, et al. Regulation of membrane-cytoskeletal interactions by tyrosine phosphorylation of erythrocyte band 3. *Blood*. 2011;117(22):5998–6006.

74. Fisher KA, Yanagimoto KC. Effect of membrane splitting on transmembrane polypeptides. *J. Cell Biol.* 1986;102(2):551–9.

75. Morrison M, Mueller TJ, Edwards HH. Protein architecture of the erythrocyte membrane. *Prog. Clin. Biol. Res.* 1981;51:17–34.

Figure legends

Figure 1. Knobs in the membrane of a *P. falciparum*-infected erythrocyte have an underlying electron-dense layer. Average of 20 slices from a tomogram of a high-pressure frozen, freeze-substituted schizont, showing knobs in the erythrocyte membrane and underlying electron-dense material. cyt, erythrocyte cytoplasm; mem, erythrocyte membrane; TVN/MC, tubulovesicular network/Maurer's cleft.

Figure 2. Knobs are visible as dark patches in electron micrographs of detergent-extracted schizont skeletons. Electron micrograph showing several knobs, indicated by arrowheads, in a negative-stained schizont skeleton, with surrounding cytoskeletal material. Inset: Two-fold enlarged view of the knob at top left.

Figure 3. Knobs contain spiral structures seen in sections through three dimensional reconstructions. A-C) Sections (averages of 3-4 slices) taken at different heights through knobs in a tomogram of a negative-stained schizont skeleton, showing a spiral structure. White arrows in A indicate some examples of radiating connections between turns; yellow arrows in C indicate diffuse coating material with a radiating pattern. D-E) Handedness and depth of knob spirals: models of two adjacent knobs from opposite sides of the skeleton, which have been collapsed onto one another during lysis and staining, viewed face-on (D) and from the side (E). F) Section through the tomogram tilted to cut through the coating layer of one side of a knob cone, showing coating material over at least five turns in curved layers

(yellow arrows). Some stain-excluding membrane material (marked in F by a dashed line; see Fig. 4B) remains after detergent extraction.

Figure 4. The electron-dense coating layer lies between the spiral and the membrane. Comparison of side-view sections through knobs in tomograms of schizont material prepared using different methods, showing layered arrangement of spiral, coat layer and membrane; averages of 10 tomographic slices through the knob apex. A) High pressure-frozen, freeze-substituted schizont showing membrane bilayer and underlying electron-dense material. B) Negative-stained detergent-insoluble schizont skeleton; contrast inverted to match A and C. The path of the spiral coil through the tomogram section is indicated by green circles. Some membrane remains after detergent extraction. View orthogonal to the plane of the tomogram. C) Schizont skeleton in vitreous ice, showing partially detergent-extracted membrane and underlying electron-dense material. A sharp discontinuity is present at the apex and in the coat layer.

Figure 5. Knob skeletons make multiple connections to the erythrocyte cytoskeleton. A) Schizont skeleton with knob skeletons in vitreous ice, average of 50 slices from an NAD-filtered cryo-tomogram. B) Uninfected erythrocyte skeleton, average of 30 slices. C) Enlarged view of boxed region in A, average of 30 slices, showing four knob skeletons and surrounding cytoskeleton. D) The same region shown in B, with superimposed model of knobs and associated material in 3D. Spiral strands are partially traced as green tubes and the coating layer of the knob skeletons is outlined by magenta contours. Points of connection with the surrounding cytoskeletal material (dark blue tubes) are marked by yellow spheres. E) Orthogonal views of a model of a typical knob skeleton (top right in C,D). In the side view (top), the estimated location of the cell membrane prior to detergent-extraction, based on

Figure 4, is marked by a dashed line. The outer surface of the coat layer has been rendered as a mesh (magenta).

Figure 6. Immuno-EM labelling of KAHRP in knob skeletons. A). Thick section (average of 50 slices) from a cryo-tomogram of schizont skeleton labelled with anti-KAHRP antibody 18.2 and 10 nm gold-conjugated secondary antibody. B) The same field of view shown in A, with 70 slices of a 3D model overlaid, describing knob spirals by the first and last turn (green contours), and gold beads as cyan spheres. C) Sections (30 slices each) through individual knobs in a cryo-tomogram of schizont skeleton labelled with mAb 18.2 and gold-conjugated secondary antibody, showing spiral structure with radiating pattern and gold labelling on the coat layer. Connected cytoskeleton is also visible. D) Model showing spirals as first and last turn (green contours) and gold label (cyan spheres) in a cryo-tomogram of schizont skeleton labelled with anti-KAHRP antibody 18.2. Dashed lines mark the boundaries in x of the volume shown in the side view. E) Chart showing the average density of gold beads at a given radial distance (in 3D) from knob spirals in four cryo-tomograms of schizont skeletons labelled with KAHRP antibody 18.2 and 10 nm gold-conjugated secondary antibody.

Figure 7. Knob membranes have a distinct distribution of membrane proteins. Cryo-scanning electron microscopy images of freeze-fractured schizont coated with 4 nm chromium, showing erythrocyte membrane proteins. The knobs are clearly recognizable as indentations (A) or protrusions (B). Membrane proteins are visible as small lighter-shaded bumps forming various patterns on the surface. A) E-face (inside of the outer membrane leaflet). B) P-face (outside of inner membrane leaflet). Knobs are indicated by white arrowheads. C) Schematic of the knob structure, showing the spiral with coat layer underlying the erythrocyte membrane, and erythrocyte spectrin connecting to the outside of the coat

layer. Membrane proteins are present at the knob apex and in the surrounding erythrocyte membrane, but are otherwise sparse in the knobs.

Figure 1

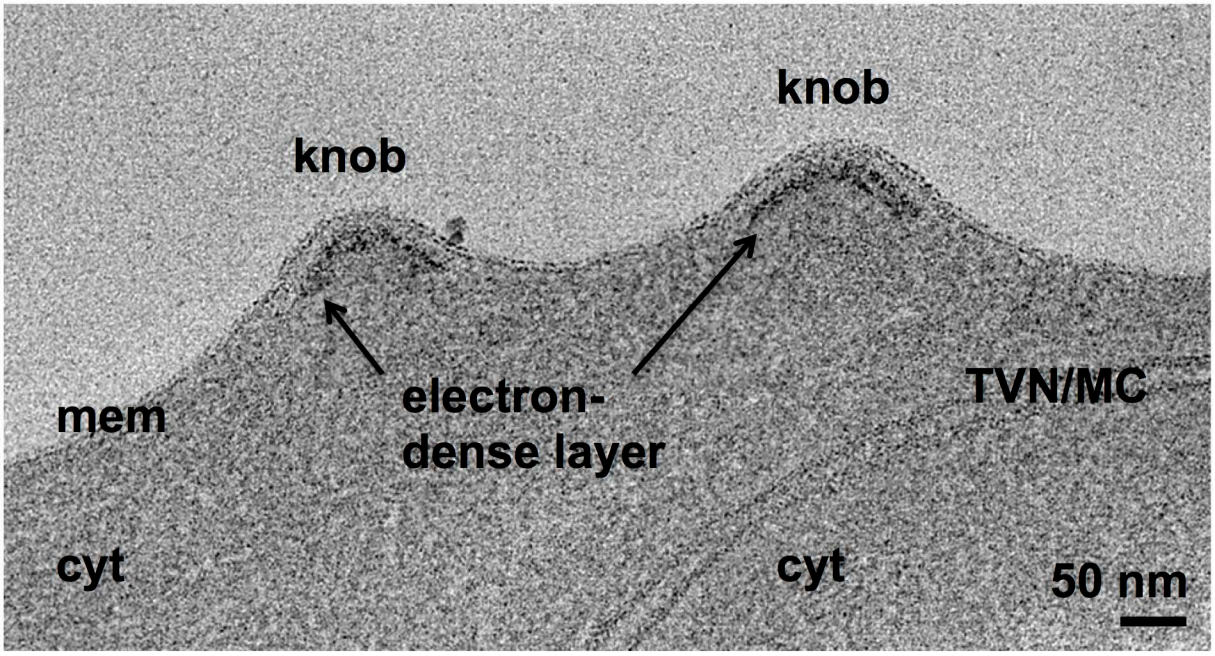

Figure 2

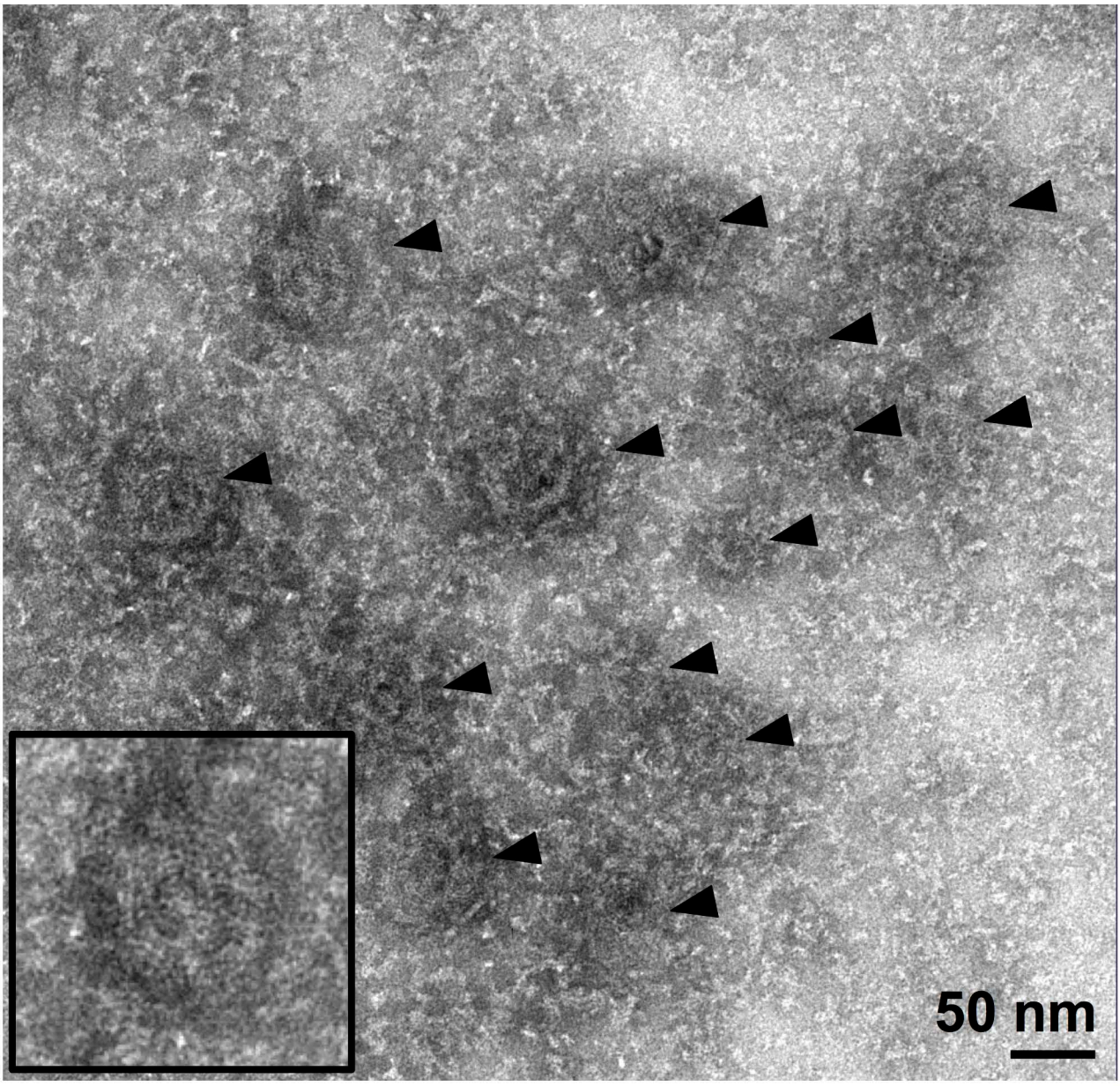

Figure 3

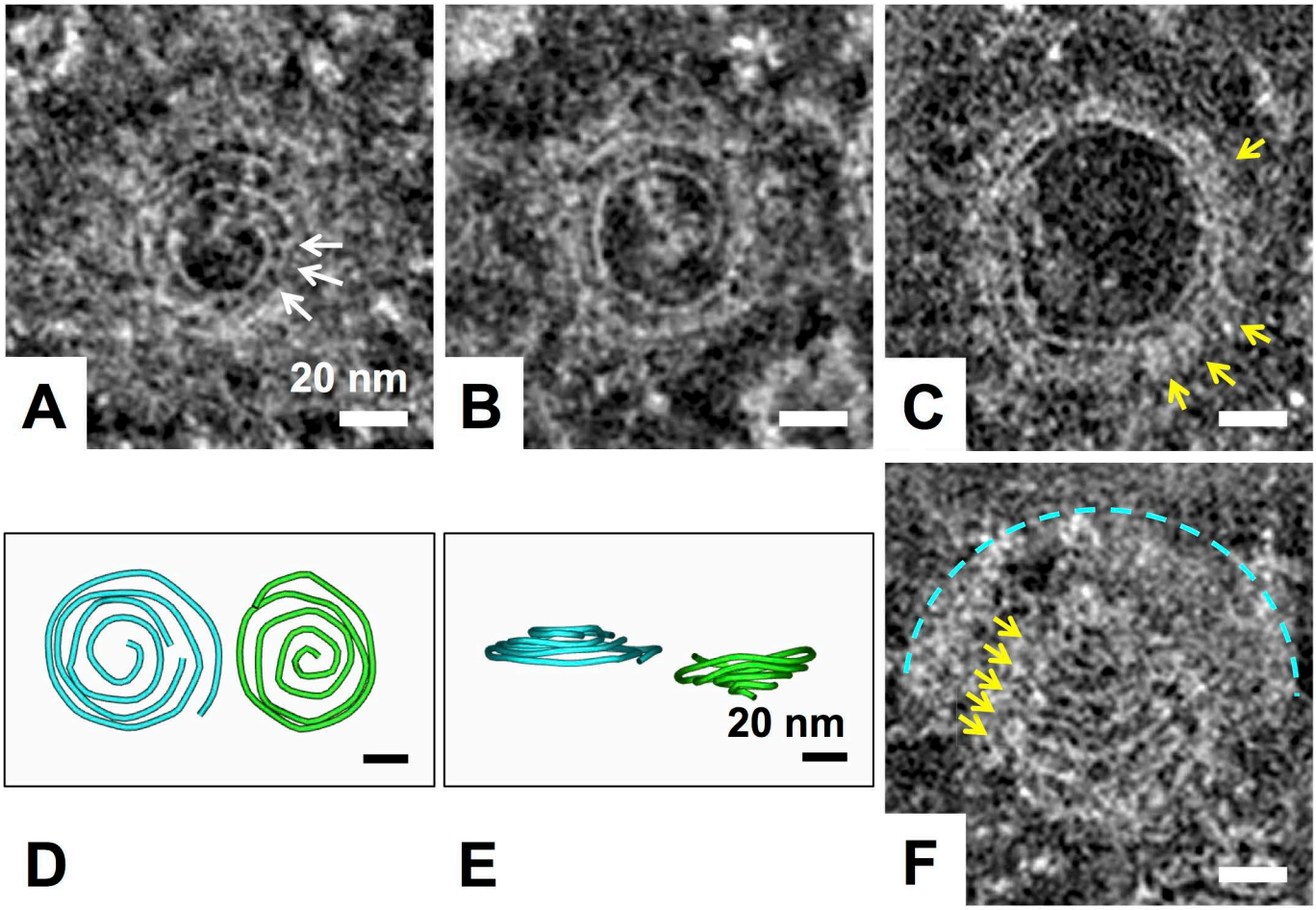

Figure 4

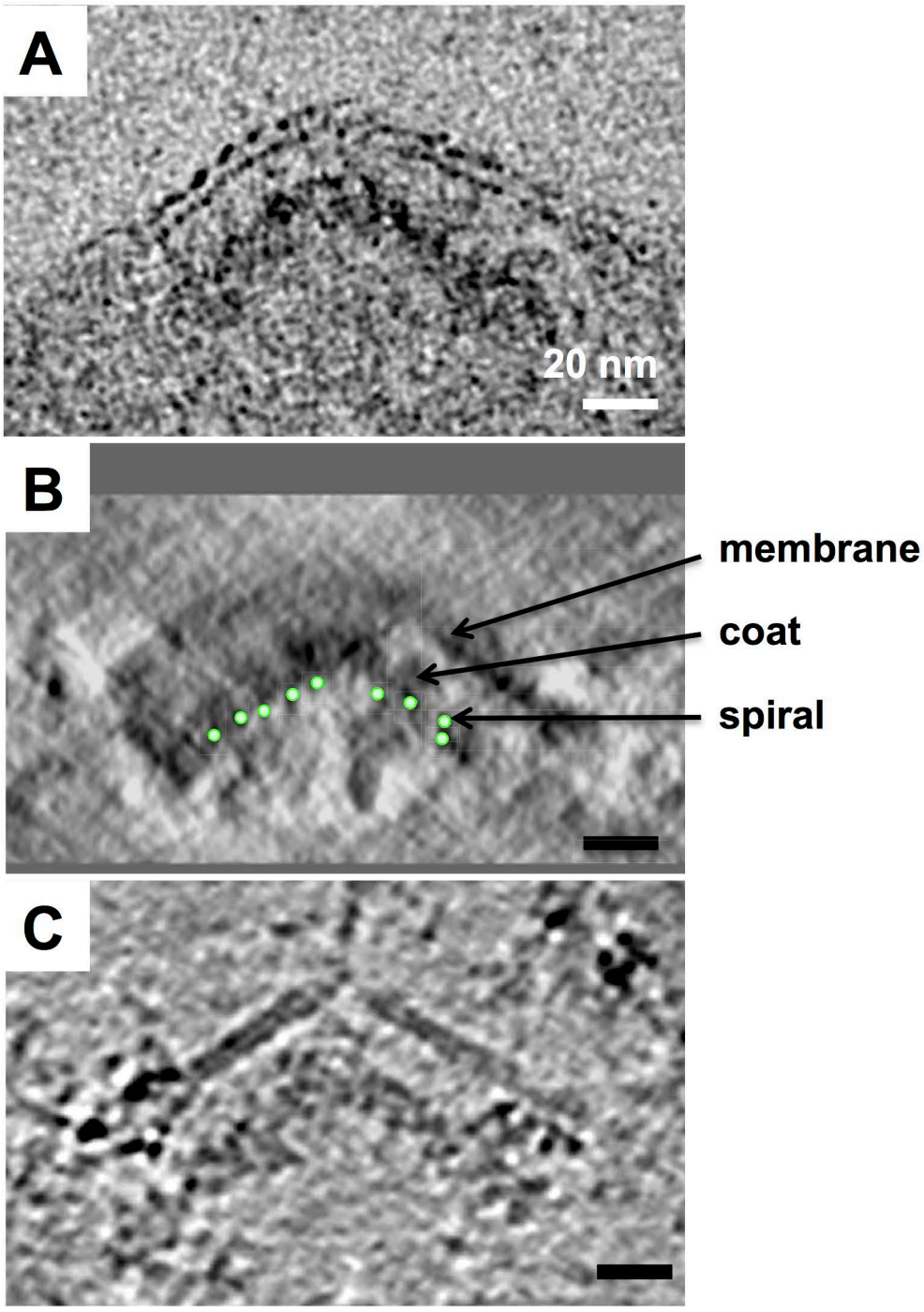

Figure 5

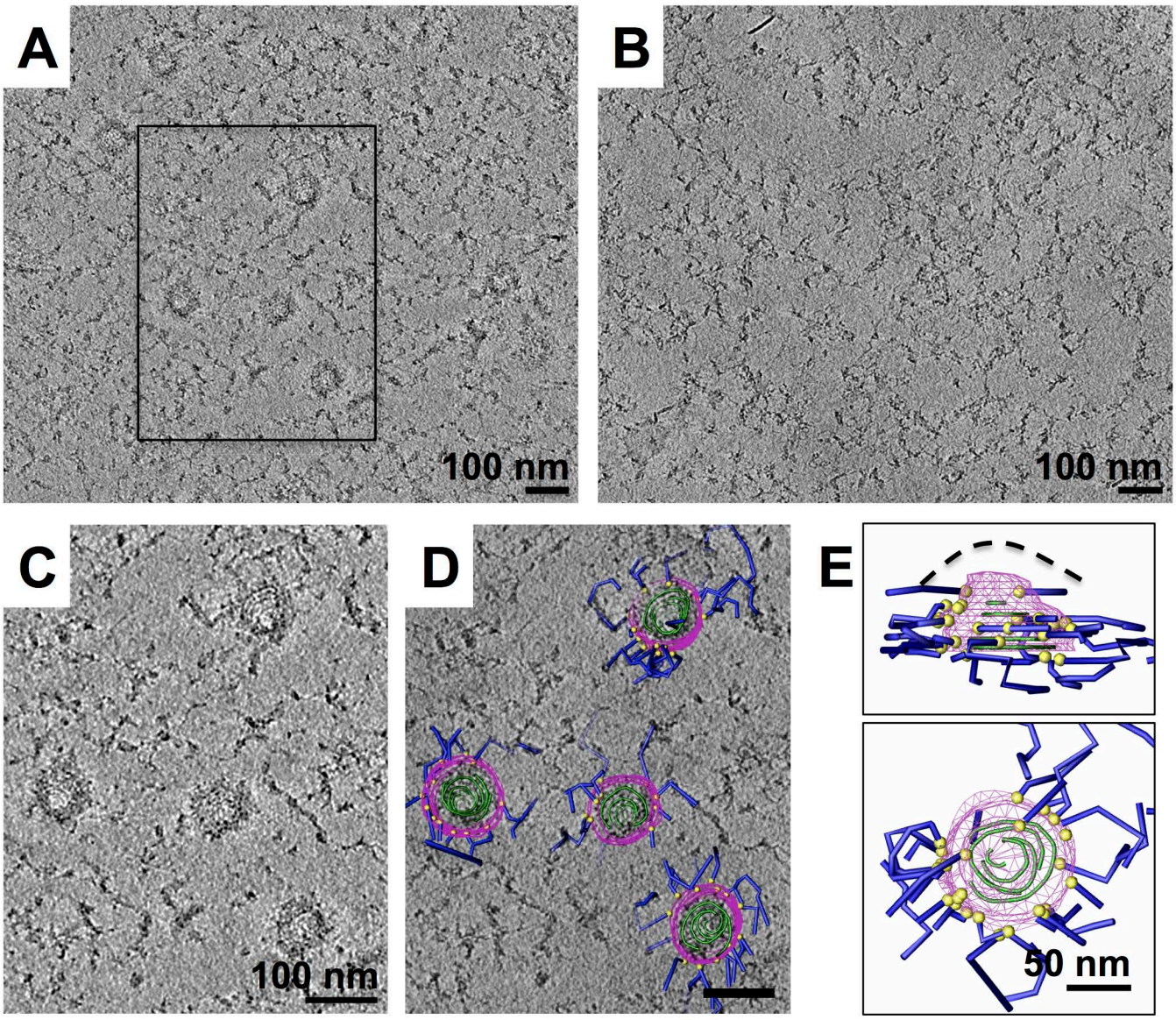

Figure 6

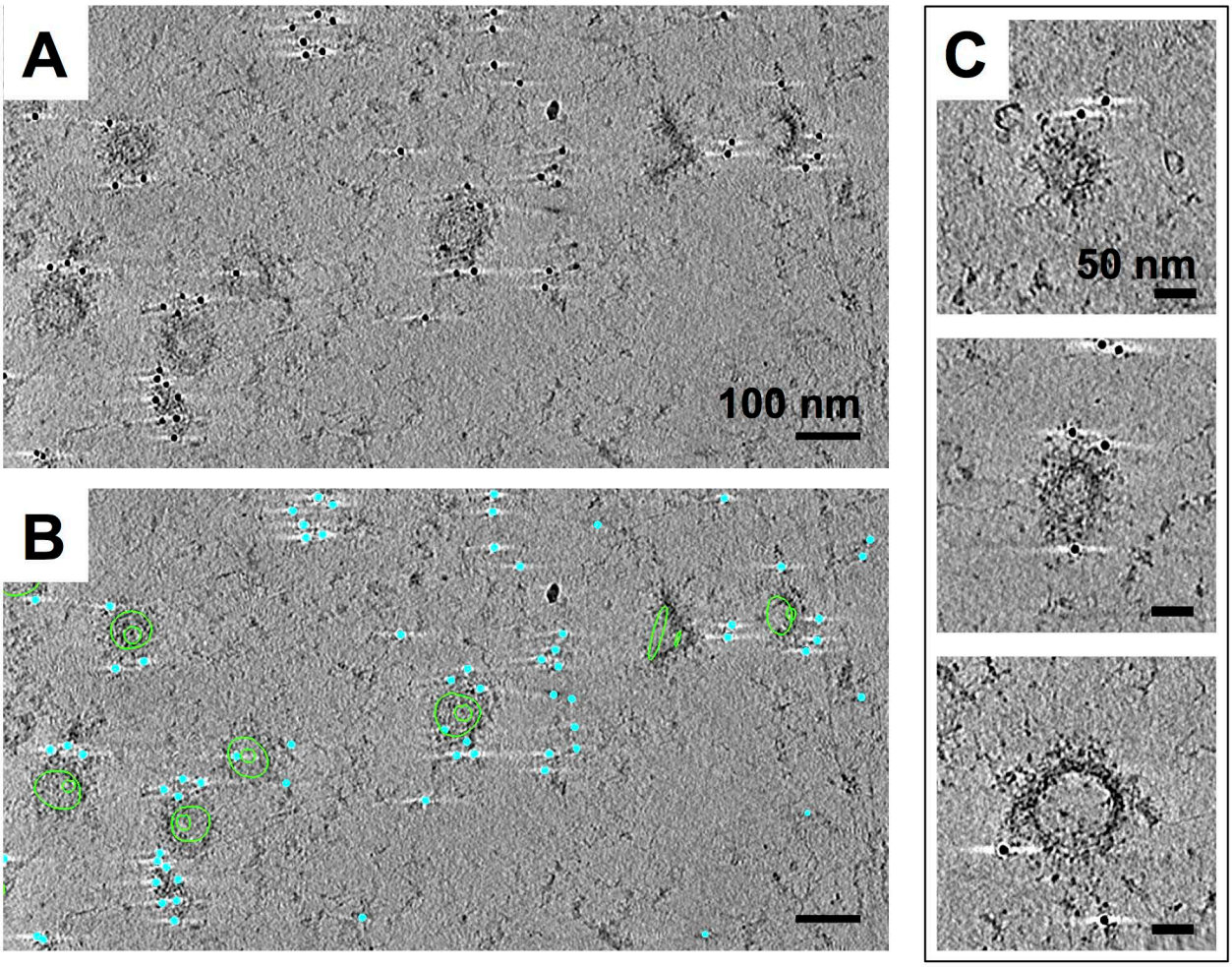
A
100 nm
B
C
50 nm

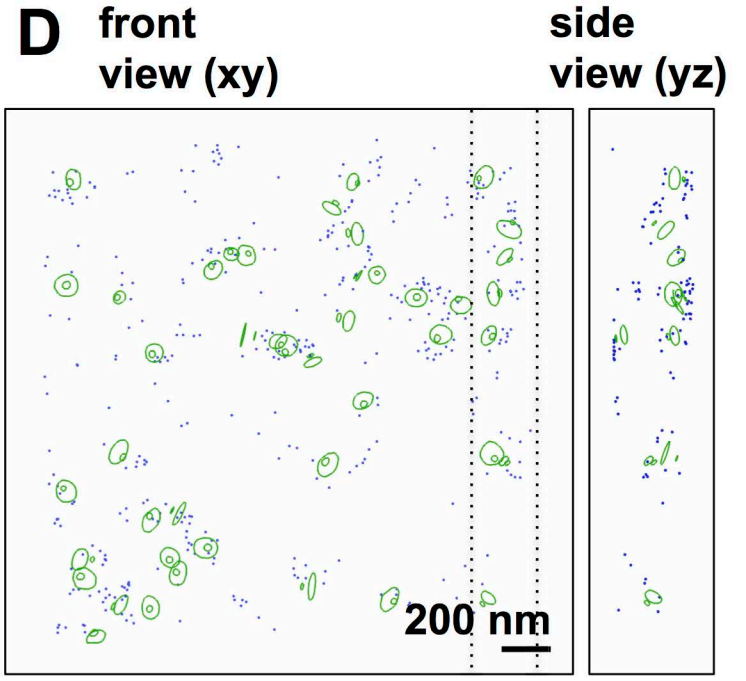
D
front
view (xy)
side
view (yz)
200 nm

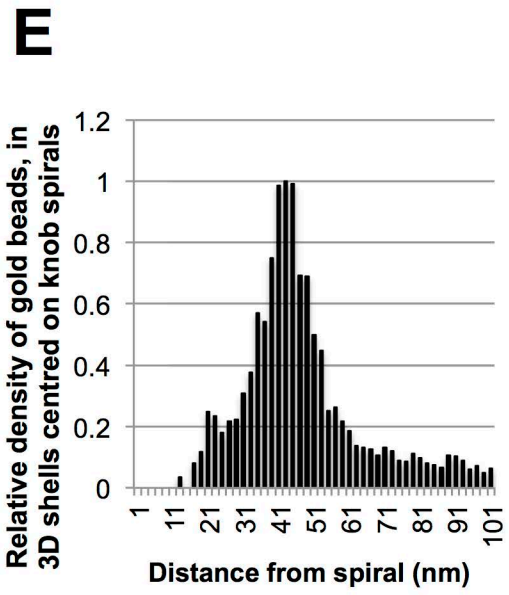
E
Relative density of gold beads, in 3D shells centred on knob spirals
1.2
1
0.8
0.6
0.4
0.2
0
1
11
21
31
41
51
61
71
81
91
101
Distance from spiral (nm)

Figure 7

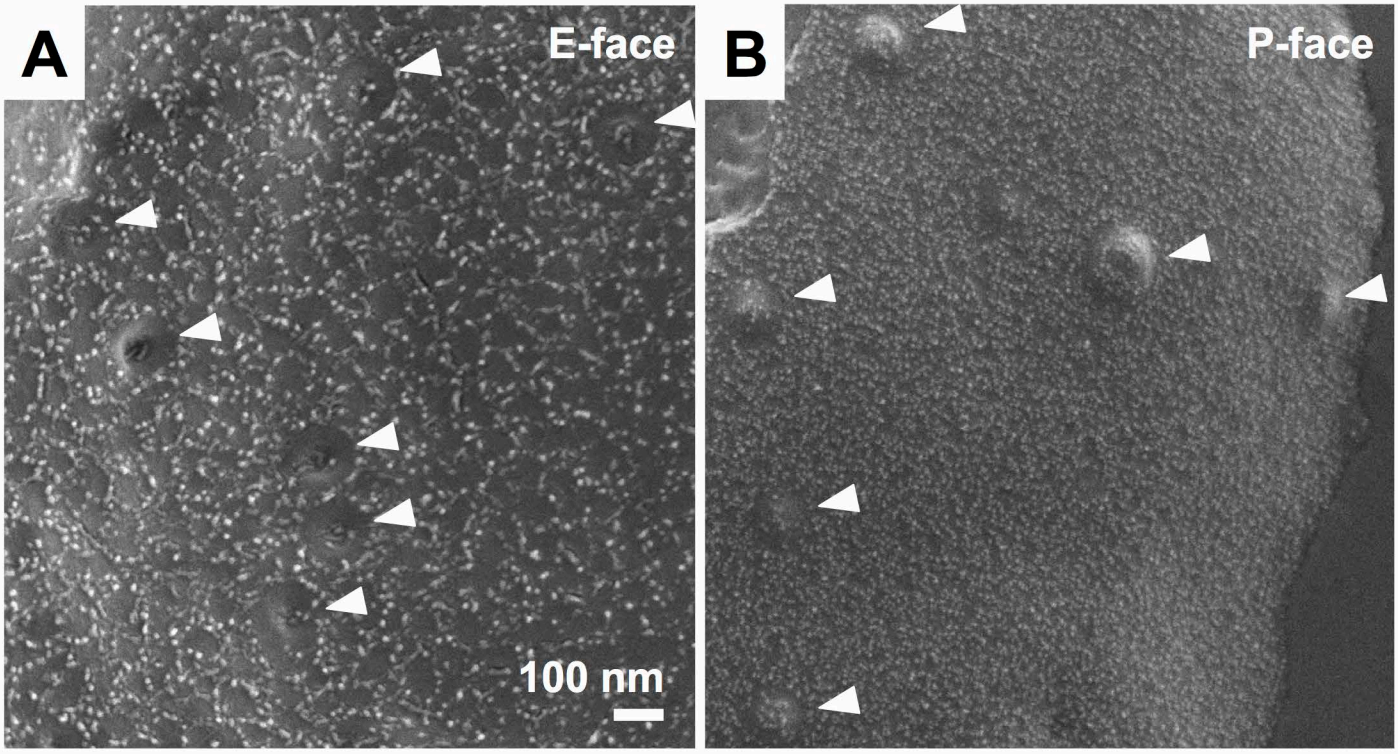
A
E-face
100 nm
B
P-face

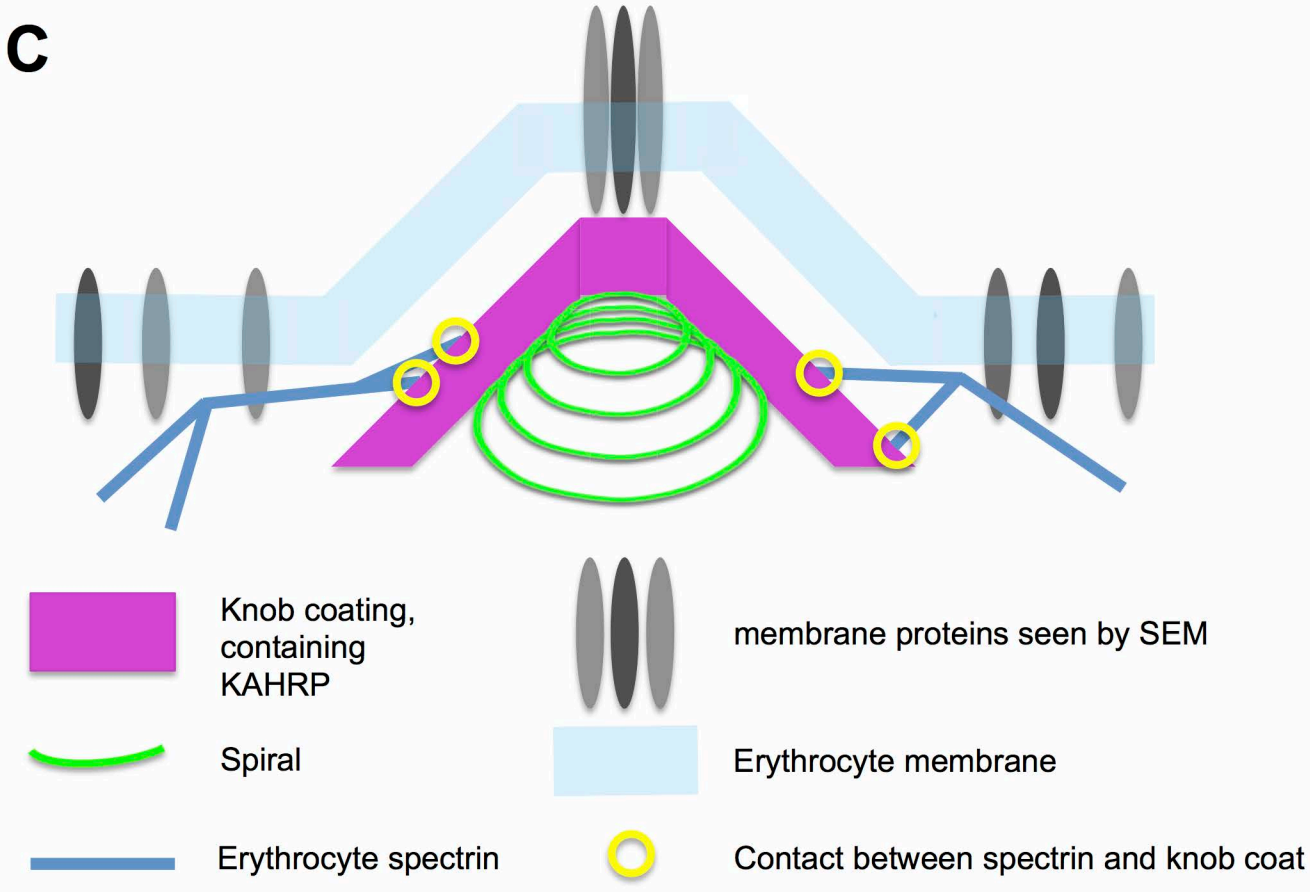
C
Knob coating, containing KAHRP
membrane proteins seen by SEM
Spiral
Erythrocyte membrane
Erythrocyte spectrin
Contact between spectrin and knob coat